Graph-Based Retinal Fluid Segmentation from OCT Images

Ipek Oguz[1,2], Li Zhang[1,3], Michael D. Abràmoff[1,2,3,4,5], and Milan Sonka[1,3,4,2]

[1]The Iowa Institute for Biomedical Imaging
[2]Department of Ophthalmology and Visual Sciences
[3]Department of Electrical and Computer Engineering
[4]Department of Biomedical Engineering
The University of Iowa, Iowa City, Iowa, USA
[5]Department of Veterans Affairs, Iowa City, USA
{ipek-oguz,li-zhang-1,michael-abramoff,milan-sonka}@uiowa.edu

Abstract. Accurate and reproducible segmentation of cysts and fluid-filled regions from retinal OCT images is an important goal for quantifying disease status, longitudinal progression and response to therapy in retinal diseases. However, segmentation of fluid-filled regions from OCT images is a challenging task due to their inhomogeneous appearance, the unpredictability of their number, size and location, as well as the intensity profile similarity between such regions and certain healthy tissue types. While machine learning techniques can be beneficial for this task, they require large training datasets and are often over-fitted to the appearance models of specific scanner vendors. We propose a knowledge-based approach that leverages a carefully designed cost function and graph-based segmentation techniques to provide a vendor-independent solution to this problem. We illustrate the results of this approach on the MICCAI 2015 OPTIMA Cyst Segmentation Challenge dataset.

Keywords: cyst segmentation, fluid-associated abnormalities, optimal multi-object segmentation, retina, OCT.

1 Introduction

Accurate and robust quantification of retinal cysts/fluid-associated abnormalities from OCT scans are important for automated assessment of disease status for age-related macular degeneration (AMD), retinal vein occlusion (RVO), and diabetic macular edema (DME). Accurate quantification techniques allow for evaluating disease progression as well as response to treatment. However, automated quantification is a challenging image processing task due to unpredictability of fluid location, fluid appearance that may be similar to certain layers of healthy tissue, as well as large variations in image characteristics and appearance between different scanner vendors.

We present a graph-based cyst/fluid-associated abnormality segmentation method that builds upon our prior work in optimal segmentation methods [17, 19, 9, 18, 12, 10, 13, 11, 14]. The graph-based methods have the attractive quality of providing the globally optimal solution with respect to the cost function definition. While prior work has

focused on machine learning techniques for learning an appropriate cost function, this method has some drawbacks. In particular, these methods are often over-fitted to the image appearance from a particular scanner with specific acquisition parameters and do not generalize well to images acquired with scanners from other vendors or even to different acquisition parameters within the same vendor. While it is possible to train machine-learning based classifiers jointly on a heterogeneous set of images, this requires much larger datasets for training (certainly more than 2 images per vendor as provided in the training dataset of this Challenge).

Instead, here we propose an expert-designed (as opposed to machine-learned) cost function that generalizes well to a variety of images. This cost function takes into account the general characteristics of the input image as well as the well-known characteristics of fluid-associated abnormalities, such as their layer-dependent properties. We illustrate the results of this approach on the OPTIMA Cyst Segmentation Challenge dataset.

2 Methods

2.1 Graph-based optimal segmentation

The key technique in our framework is graph-based optimization for image segmentation [10, 7, 6, 4]. Given a cost function and a set of constraints that provides spatial context between neighboring vertices as well as neighboring surfaces and objects, graph-based techniques can be used to obtain the globally optimal segmentation solution in low-order polynomial time.

Variants of this approach have been successfully applied to many medical image analysis tasks, such as knee cartilage segmentation [17], brain [14] and cortical surface segmentation [12, 13, 11], etc. In the ophthalmic imaging domain, we have shown that graph-based LOGISMOS techniques can be used, among other things, to successfully segment the retinal tissue layers [9] and the choroid [18, 19].

2.2 Optimal retinal mask segmentation

An important pre-processing task for the retinal fluid segmentation is the determination of a retinal mask for the input image. This is important as the fluid appears dark in OCT images just like the background, and it is therefore necessary to discard all such "background" locations in order to avoid false positives in the fluid segmentation results. While our publicly available Iowa Reference Algorithms [5, 1, 10, 9, 15, 3] provide excellent accuracy and robustness for the segmentation of 11 retinal tissue layers (which can be combined to create a retinal mask) for images of eyes not exhibiting disease-related changes to layer topology, the pathological eyes that contain fluid-associated abnormalities can often be problematic, especially when these are close to the retinal boundary.

We use a two-stage approach to address this issue. First, we employ a new retinal segmentation method that focuses on segmentation of fewer layers but generates a more reliable retinal mask even in the presence of fluid-associated abnormalities. Second, we

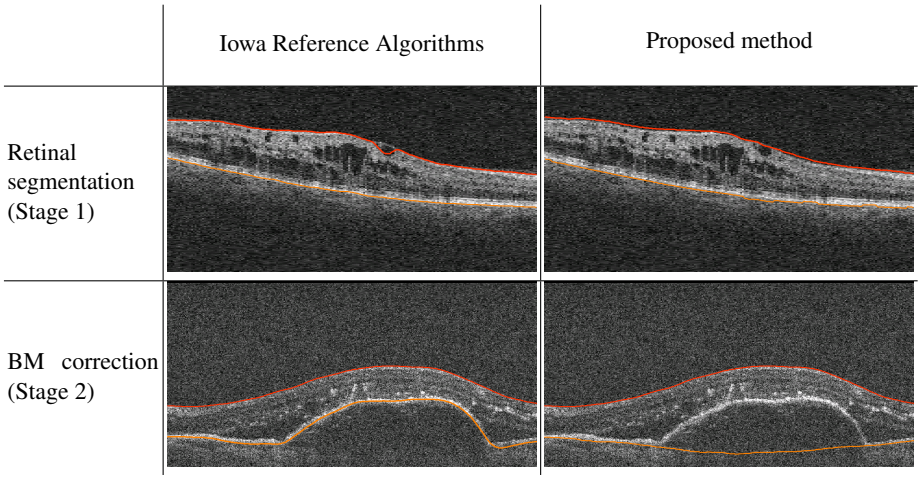

Fig. 1. The performance of the proposed two-stage optimal retinal mask segmentation algorithm in retinas containing fluid-associated abnormalities. *Left*, results from the original Iowa Reference Algorithms [5, 1, 10, 9, 15, 3]. *Right*, results from proposed method.

use our existing method for correcting the Bruch's membrane (BM) in the presence of serous pigment epithelial detachments (PED's) [18]. Fig. 1 illustrates the effect of these two stages.

The layer segmentation results obtained in this step are used both individually, in order to determine the layer membership for the layer-dependent fluid cost function parameters, as well as combined together to create a retinal mask. The rightmost column in Fig. 3 illustrates the layers used for this manuscript. We note that the number and properties for these layers were chosen based solely on the image appearance properties and the usefulness of the layer distinction for the purposes of the SEAD detection/segmentation task, rather than following clinically relevant tissue layer definitions.

2.3 Optimal fluid-associated abnormality segmentation

While the framework for the optimal fluid-associated abnormality segmentation is similar to the generic volumetric graph-based segmentation approaches [4, 10], we designed sophisticated cost functions to capture the expert domain knowledge regarding retinal fluid-associated abnormalities. This is in contrast to our previous work [16, 5] that leverages machine learning techniques to automatically deduct the cost function based on a training set.

The manually designed cost function reflects the known properties of the SEAD's as seen in retinal OCT images in a layer-specific manner. Additionally, to account for the changes of appearance of the healthy retinal tissue in images acquired by OCT scanners from different manufacturers, retinal tissue characteristics are determined directly from the image based on the retinal mask segmentation and the knowledge of relative intensities between different layers, rather than enforcing a priori intensity models. For

this purpose, Mahalanobis distances are used as the cost function using the intensity distribution parameters $\mu(l)$ and $\sigma(l)$ determined for each layer l.

$$C_m(x, l(x)) = \frac{I(x) - \mu(l(x))}{\sigma(l(x)} * 100 \tag{1}$$

An important concern for fluid-associated abnormality segmentation is the image intensity similarity between the fluid regions and the healthy tissue layers with dark appearances. To differentiate between these two classes of "dark" image locations, we use a generalization of Frangi's vesselness measure [8] to the enhancement of higher-order structures [2], in this particular case, to a "sheetness" measure. Given a 3D image, image locations that belong to a 2D plate of dark intensities compared to their neighborhood respond strongly to this filter, similar to the vesselness filter that generates a strong response in image locations that belong to a 1D tubular structure. The "sheetness" measure is computed in a multi-scale manner to determine the maximum filter response. In our framework, this "sheetness" measure is used to distinguish dark image intensities that belong to blob-like fluid pockets from sheet-like healthy tissue layer. As in [2], we define the sheetness at a scale σ as follows:

$$C_s(x, \lambda(x))_\sigma = (1 - e^{-\frac{R_A^2}{2\alpha^2}}) \times e^{-\frac{R_B^2}{2\beta^2}} \times (1 - e^{-\frac{s^2}{2\gamma^2}}) \tag{2}$$

$$R_A = \frac{|\lambda_{M+1}|}{\prod_{i=M+2}^{N} |\lambda_i|^{\frac{1}{N-M-1}}} \tag{3}$$

$$R_B = \frac{|\lambda_M|}{\prod_{i=M+1}^{N} |\lambda_i|^{\frac{1}{N-M}}} \tag{4}$$

$$S = \sqrt{\sum_{j=1}^{N} \lambda_j^2} \tag{5}$$

In this formulation, N is the dimensionality of the image ($N = 3$), M is the dimensionality of the object being enhanced ($M = 2$ for sheetness, $M = 1$ for vesselness), λ's are the eigenvalues of the Hessian matrix at the current scale σ, S is the Frobenius norm of the Hessian matrix and α, β, γ are the relative weights.

A final component of the cost function is designed to distinguish between convex-shaped fluid pockets from more widespread fluid-associated abnormalities, especially sub-retinal fluid, which may appear as thick bands of dark image patches, which are not "healthy" tissue but do not necessarily form blob-like structures. The OPTIMA Cyst Segmentation Challenge ground truth segmentations often do not consider these latter regions to be part of the fluid segmentation. The sheetness filter often produces similar response for these two types of regions and therefore cannot adequately distinguish between them. For this purpose, we incorporated a third cost function component using the 1-D gradient response in the horizontal directions in the b-scans at a coarse level of resolution.

As the OPTIMA Challenge does not consider serous pigment epithelial detachments (PED's), even though these also are fluid-associated abnormalities, these regions were pre-segmented using [18] and masked from the cost function.

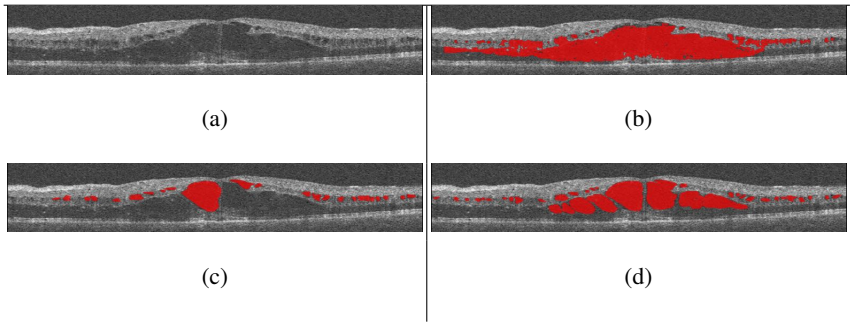

Fig. 2. In areas where there are thick bands of fluid-filled regions, the distinction between a blob-like cyst and other types of fluid-associated abnormalities becomes ambiguous even for the expert-provided "truth". (a) Raw OCT image. (b) Our segmentation result. (c) Ground truth provided by expert 1. (d) Ground truth provided by expert 2.

A standard Boykov graph cut was used for optimizing the segmentation. A weighted sum of the three cost function components described above, i.e., the layer-dependent Mahalanobis intensity distance, the sheetness measure and the 1-D gradient filter, was used to determine the node costs, whereas the image intensity differences between neighboring voxels, weighted by the spatial distances of the voxel locations (i.e., the image resolution), was used as the edge costs. The weights of the three cost components were set on a per-layer basis to encode known characteristics of the retina and fluid-associated abnormalities; for example, the thick band of fluid is far more likely to occur next to the outer retina than elsewhere, and the sheetness measure is more relevant in dark layers rather than in bright layers.

3 Experimental Methods

Dataset. The OPTIMA Cyst Segmentation Challenge data consisted of a training dataset (15 scans) and two testing datasets (8 and 7 scans, respectively). The images were acquired with devices from 4 different vendors (Spectralis, Cirrus, Topcon and Nidek) and represented a relatively wide range of acquisition characteristics.

Segmentation parameters. All parameters for the proposed segmentation algorithm were empirically set in a vendor-independent manner, based on performance on the entire training dataset.

4 Results

Fig. 3 shows an illustrative example from each vendor in the Challenge dataset. We note that the algorithm produces satisfactory segmentation results in each image despite the widely differing image appearances across scanner vendors as well as the different pathologies present in each retina.

5 Discussion

Our retinal fluid-associated abnormality segmentation algorithm relies on expert-designed cost functions. This knowledge-based segmentation approach has several advantages compared to typical machine learning approaches such as [16, 5], as our approach is not dependent on the appearance models of specific training data and does not require large sets of manual annotations for initial training. As such, it is more generalizable and readily applicable to a variety of OCT scans of retinas at different disease stages and images acquired with different scanners. An additional strength of our method is that it allows the segmentation of not only small pockets of fluid but rather all fluid-associated abnormalities, including PED's, subretinal fluid and diffuse abnormalities, which may be relevant for clinical studies.

The segmentation quality of the fluid-associated abnormalities from healthy tissue in the training dataset was satisfactory in for all vendors. The distinction between the blob-like fluid pockets and other fluid-associated abnormalities was overall good, even though for a few images in the training dataset, our algorithm generated false positive responses in some of the larger bands of fluid. We note that the differences between these two types of fluid abnormalities are often subtle and rather subjective (as evidenced by the relatively large inter-rater variability in such regions in the challenge ground truth), as illustrated in Fig. 2. In this example, while our automated segmentation result does not agree perfectly with either expert's manual annotation, we observe that "the truth" is quite ambiguous. We are further exploring the fine-tuning of our cost function with respect to this aspect of the segmentation task. However, we also note that since both types of structures represent pathology which are difficult to differentiate from each other in OCT images even for medical experts, it may be clinically more beneficial to segment all such regions together to improve the reliability/reproducibility of the image quantification results (for both automated and manual measurements).

6 Conclusion

Our algorithm is a highly generalizable knowledge-based approach that leverages graph theoretic segmentation techniques. The careful design of cost functions makes it applicable to a wide variety of image appearances and removes the need for large training datasets, which are labor-intensive to create.

7 Acknowledgements

We are grateful to Yuri Boykov for insightful discussions. This research was supported in part by NEI awards R01EY019112 and R01EY018853, NIBIB award R01EB004640, and the Arnold and Mabel Beckman Initiative for Macular Research.

References

1. Abràmoff, M.D., Garvin, M.K., Sonka, M.: Retinal imaging and image analysis. IEEE Reviews in Biomedical Engineering 3, 169–208 (2010)

2. Antiga, L.: Generalizing vesselness with respect to dimensionality and shape. Insight Journal (Aug 2007)
3. Antony, B., Abràmoff, M.D., Tang, L., Ramdas, W.D., Vingerling, J.R., Jansonius, N.M., Lee, K., Kwon, Y.H., Sonka, M., Garvin, M.K.: Automated 3-D method for the correction of axial artifacts in spectral-domain optical coherence tomography images. Biomedical optics express 2(8), 2403–2416 (Aug 2011)
4. Boykov, Y., Kolmogorov, V.: An Experimental Comparison of Min-cut/Max-flow Algorithms for Energy Minimization in Vision. IEEE transactions on Pattern Analysis and Machine Intelligence 26(9), 1124–1137 (Sep 2004)
5. Chen, X., Niemeijer, M., Zhang, L., Lee, K., Abràmoff, M.D., Sonka, M.: Three-dimensional segmentation of fluid-associated abnormalities in retinal OCT: probability constrained graph-search-graph-cut. IEEE Transactions on Medical Imaging 31(8), 1521–1531 (Aug 2012)
6. Delong, A., Boykov, Y.: Globally optimal segmentation of multi-region objects. International Conference on Computer Vision (2009)
7. Delong, A., Osokin, A., Isack, H.N., Boykov, Y.: Fast Approximate Energy Minimization with Label Costs. International Journal of Computer Vision 96(1), 1–27 (Jul 2011)
8. Frangi, A.F., Niessen, W.J., Vincken, K.L., Viergever, M.A.: Multiscale vessel enhancement filtering. Medical Image Computing and Computer-Assisted Intervention MICCAI pp. 130–137 (1998)
9. Garvin, M.K., Abràmoff, M.D., Wu, X., Russell, S.R., Burns, T.L., Sonka, M.: Automated 3-D intraretinal layer segmentation of macular spectral-domain optical coherence tomography images. IEEE Transactions on Medical Imaging 28(9), 1436–1447 (Sep 2009)
10. Li, K., Wu, X., Chen, D.Z., Sonka, M.: Optimal surface segmentation in volumetric images–a graph-theoretic approach. IEEE Transactions on Pattern Analysis and Machine Intelligence 28(1), 119–134 (Jan 2006)
11. Oguz, I., Sonka, M.: LOGISMOS-B: layered optimal graph image segmentation of multiple objects and surfaces for the brain. IEEE Transactions on Medical Imaging 33(6), 1220–1235 (Jun 2014)
12. Oguz, I., Sonka, M.: Robust cortical thickness measurement with LOGISMOS-B. Medical image computing and computer-assisted intervention : MICCAI 17(Pt 1), 722–730 (2014)
13. Oguz, I., Styner, M., Sanchez, M., Shi, Y., Sonka, M.: LOGISMOS-B for Primates: Primate Cortical Surface Reconstruction and Thickness Measurement. Proceedings of SPIE Medical Imaging 9413, 941313–941313–6 (2015)
14. Oguz, I., Zhang, H., Rumple, A., Sonka, M.: RATS: Rapid Automatic Tissue Segmentation in rodent brain MRI. Journal of neuroscience methods 221, 175–182 (Jan 2014)
15. Quellec, G., Lee, K., Dolejsi, M., Garvin, M.K., Abràmoff, M.D., Sonka, M.: Three-dimensional analysis of retinal layer texture: identification of fluid-filled regions in SD-OCT of the macula. IEEE Transactions on Medical Imaging 29(6), 1321–1330 (Jun 2010)
16. Xu, X., Lee, K., Zhang, L., Sonka, M., Abramoff, M.: Stratified Sampling Voxel Classification for Segmentation of Intraretinal and Subretinal Fluid in Longitudinal Clinical OCT Data. IEEE Transactions on Medical Imaging (Mar 2015)
17. Yin, Y., Zhang, X., Williams, R., Wu, X., Anderson, D.D., Sonka, M.: LOGISMOS–layered optimal graph image segmentation of multiple objects and surfaces: cartilage segmentation in the knee joint. IEEE Transactions on Medical Imaging 29(12), 2023–2037 (Dec 2010)
18. Zhang, L., Buitendijk, G.H.S., Lee, K., Sonka, M., Springelkamp, H., Hofman, A., Vingerling, J.R., Mullins, R.F., Klaver, C.C.W., Abràmoff, M.D.: Validity of Automated Choroidal Segmentation in SS-OCT and SD-OCT. Investigative Ophthalmology & Visual Science 56(5), 3202–3211 (May 2015)
19. Zhang, L., Lee, K., Niemeijer, M., Mullins, R.F., Sonka, M., Abràmoff, M.D.: Automated segmentation of the choroid from clinical SD-OCT. Investigative Ophthalmology & Visual Science 53(12), 7510–7519 (Nov 2012)

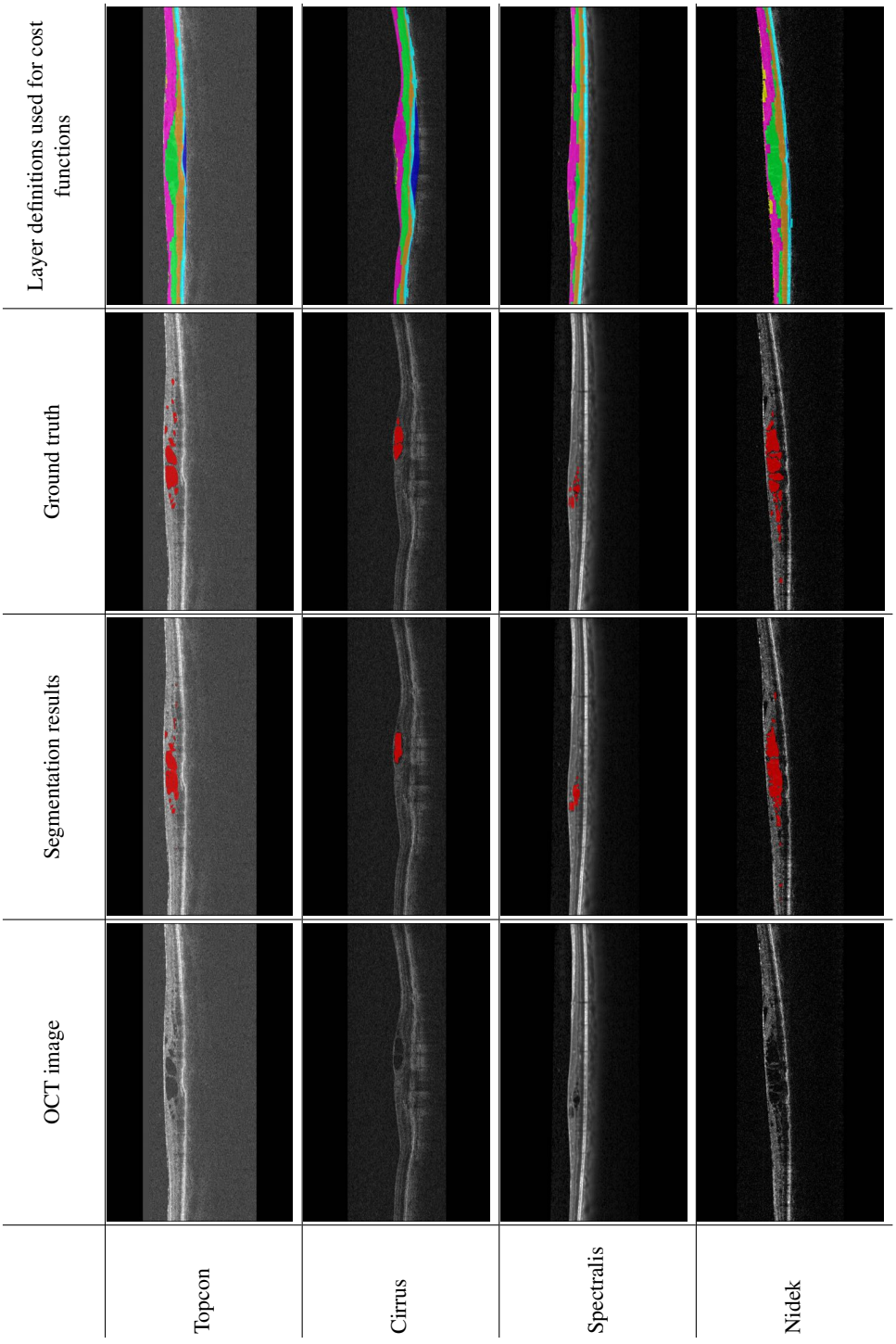

Fig. 3. The performance of the proposed algorithm in retinas containing fluid-associated abnormalities, illustrated with images acquired with scanners from different vendors.